CrossMark

Microscale phase separation condensers with varied cross sections of each fluid phase: Heat transfer enhancement and pressure drop reduction

Xiongjiang Yu, Jinliang Xu *, Jindou Yuan, Wei Zhang

The Beijing Key Laboratory of Multiphase Flow and Heat Transfer for Low Grade Energy Utilization, North China Electric Power University, Beijing 102206, PR China

ABSTRACT

Micro-condenser using the phase separation concept was investigated in this paper. Lined pin fin arrays generate liquid passages and vapor passages alternatively in chip width direction. The decreased Gibbs free energy with gas–liquid interface advancing pin fin throat location is the mechanism to induce liquid flow from vapor passages to liquid passages. The decreased energy dissipation due to decreased interfacial area between the two phases accounts for pressure drop reduction. Three micro-condensers were investigated: microchannel condenser (SWM), parallel phase separation condenser (PPS with constant cross sections of fluid passages) and conical phase separation condenser (CPS with varied cross sections of fluid passages). Micro-condensers had identical project condensation surface of 25.0 mm by 3.0 mm. The etched depth was 75 μm. Water-vapor was the working fluid. Compared with SWM, phase separation condensers increased mass flow rate by 15% at similar pressure drops. PPS condenser enhances heat transfer at moderate or smaller cooling intensity, but deteriorates heat transfer at large condensed liquid flow rate, at which over liquid expansion occurs to flood all pin fin side walls. CPS condenser self-adapts variations of flow rates of the two phases to stabilize vapor–liquid interface near pin fin membrane. Pin fin side walls facing vapor passage are covered by thin liquid film to eliminate over liquid expansion. CPS condenser enhances heat transfer over entire operating parameter ranges, increasing condensation heat transfer coefficients by 74% maximally while pressure drops are decreased. CPS condenser has the best performance among the three condensers.

© 2017 Elsevier Ltd. All rights reserved.

1. Introduction

Chen et al. [1] published first paper of phase separation tube for large size condensers in 2012. The tube cross section is divided into a core region and a near wall region, which are interfaced by a membrane separator. Condensed liquid is captured by the membrane separator and flows in the core region. Vapor is resisted by the separator to flow in the near wall region. Thus, condenser tube wall is covered by ultra-thin liquid film to enhance heat transfer.

Mesh screen with micro-pores was the separator material [1]. The phase separation effect was verified using a horizontal air-water flow system. The tube had an inner diameter of 13.08 mm and a length of 2.5 m. A 9.32 mm diameter mesh cylinder, acting as the membrane separator, was suspended in the tube. Mesh pore size was ~100 μm. Experiments showed that at small liquid content of the two-phase mixture, all liquids are collected by mesh

cylinder and flow inside, air flows in the near wall region, which is called the full separation mode. At large liquid content of the two-phase mixture, mesh cylinder collects part of liquid, but the tube surface area covered by gas is significantly increased, which is called the partial separation mode.

Subsequently, experiments were performed on phase separation tube [2,3]. The separation effect is also effective for vertically positioned tube [4]. The liquid film thickness can be decreased to 1/6–1/3 of that in a bare tube without inserting a membrane separator [5]. Xie et al. [6] reported condensation heat transfer in a horizontal tube with a 14.81 mm diameter and a 1200 mm length, by suspending a membrane separator, which was formed by packaging two layers of mesh screen surfaces [7]. Measurements showed that phase separation condenser tube can have condensation heat transfer coefficients of more than two times of those in a bare tube, maximally. Meanwhile, the total thermal resistance was decreased by 45.6%, maximally.

Here, the phase separation tube for large size condensers is extended to micro-condensers, having wide applications in

Nomenclature

A	interface area (m^2)
A_c	cross sectional area of flow passages over the entire condenser width (m^2)
$A_{c,l}$	cross sectional area of liquid passages over the entire condenser width (m^2)
$A_{c,v}$	cross sectional area of vapor passages over the entire condenser width (m^2)
A_p	channel cross sectional area (m^2)
A_s	projected surface area of a droplet (m^2)
A_t	total side wall area of pin fins (m^2)
a	ratio of all droplets surface area to the two-phase mixture volume (m^{-1})
C_d	drag coefficient of a droplet in a flowing vapor
Co	confinement number
d_d	droplet diameter (m)
d_p	channel hydraulic diameter (m)
E	energy dissipation (W)
E_{lg}	energy dissipation due to interaction between two-phases (W)
$E_{tp,w}$	energy dissipation for interaction between two-phase mixture and wall (W)
F_d	frictional force between vapor and droplet (N)
$F_{tp,w}$	frictional force between two-phase mixture and channel wall (N)
G	mass flux (kg/m^2 s)
$G_{Gibbs,c}$	constant parameter of Gibbs free energy (J)
G_{Gibbs}	Gibbs free energy (J)
H_e	etched depth (μm)
h	condensation heat transfer coefficient (W/m^2 K)
k	copper thermal conductivity (W/m K)
L	curvature radius at the initial location at t_1 (m)
L_c	channel length (m)
l_c	capillary length (m)
l_1	wetting length (μm)
m	mass flow rate (g/s)
m_c	cooling water flow rate (g/s)
N_d	number of droplets
O	initial curvature center point
O'	curvature center point at $t = t_2$
P	pressure (Pa)
$P_{e,l}$, $P_{e,v}$	exit pressures in liquid passage and vapor passage, respectively (Pa)
P_{in}	upstream pressure of micro-condenser (Pa)
P_l	pressure in liquid passage (Pa)
$P_{l,a}$	pressure in liquid passage for interface deviating from pin fin membrane (Pa)
$P_{l,c}$	pressure in liquid passage of CPS condenser with interface near pin fin (Pa)
$P_{l,i}$	pressure in liquid passage assuming vapor-liquid interface near pin fin (Pa)
$P_{l,p}$	pressure in liquid passage of PPS condenser with interface near pin fin (Pa)
P_v	pressure in vapor passage (Pa)

$P_{v,a}$	pressure in vapor passage for interface deviating from pin fin (Pa)
$P_{v,c}$	pressure in vapor passage of CPS condenser with interface near pin fin (Pa)
$P_{v,i}$	pressure in vapor passage assuming vapor-liquid interface near pin fin (Pa)
$P_{v,p}$	pressure in vapor passage of PPS condenser with interface near pin fin (Pa)
ΔP	pressure drop across condenser (Pa)
ΔP_{CPS}, ΔP_{PPS}	pressure difference between vapor passage and liquid passage for CPS and PPS condenser, respectively (Pa)
q	heat flux (kW/m^2)
Re	Reynolds number
r_1	radius of interface at $t = t_1$ (μm)
S_2	exposed surface area (μm^2)
T	temperature (°C)
$T_{sat,i}$	saturation temperature at each section center (°C)
$T_{w,i}$	wall temperature at the top surface of the copper block (°C)
t	time (s)
t_1	initial time before wetting (s)
t_2	time when the interface travels a distance of l_1 (s)
V	vacuum volume not occupied by solid structure (μm^3)
v	velocity (m/s)
v_m	velocity of two-phase mixture (m/s)
v_s	slip velocity between liquid and vapor (m/s)
W_n	total width at narrowed location along the flow direction (m)
x, y, z	copper height direction, chip width direction and axial flow direction (m)
z_e	exit location

Greek symbols

α	half of vertex angle of arc-shaped interface (rad)
β	volume ratio of the vapor phase to the two-phase mixture
θ	contact angle between water and silicon (rad)
η	thermal efficiency
γ	surface tension (N/m)
ρ	density (kg/m^3)
τ_{tp-w}	shear stress between two-phase mixture and channel wall (N/m^2)

Subscripts

CPS	conical phase separation condenser
g, l, v, s	gas phase, liquid phase, vapor phase and solid phase, respectively
i	section number
in	condenser inlet
out	condenser outlet
PPS	parallel phase separation condenser
SWM	solid wall microchannel condenser
1, 2, 3	regions in the copper block

compact energy and power systems. For example, micro-condenser is an important component of loop heat pipe. It is also a key component of compact refrigeration or heat pump system, dissipating heat to environment for electronic cooling applications.

Wall effect is important in small channels [8]. Capillary length l_c is defined as $l_c = \sqrt{\frac{\gamma_{lg}}{g \Delta \rho}}$. For vapor-water system, l_c is ∼2.5 mm. Droplet confinement number Co is $Co = l_c/d_p$. In microchannels, Co is much larger than 1.0, yielding droplet confinement effect to block

channel. The scale effect makes it more difficult to remove liquid. How to remove condensed liquid is a big issue.

Table 1 lists condensation heat transfer studies published in open literature [9–22]. Physically, condensation heat transfer is related to flow patterns [9]. Liquid film condensation and dropwise condensation are two frequently encountered modes [10,19]. For film condensation, liquid film separates cold wall and vapor core to dominate heat transfer [16,17]. Many factors such as capillary number, contact angle and heat flux influence the liquid film thick-

Table 1
Microscale condensation studies in the literature.

Reference	Micro-condenser test section	Working fluid	Findings and comments
Garimella [9]	Parallel channels with 400 μm < d_p < 4910 μm, channel cross section shape is circular, square, rectangular, triangular and trapezoidal	R134a	Intermittent and annular flow regimes become important for decreased hydraulic diameter
Chen and Cheng [10]	Trapezoidal silicon parallel channels with d_p = 75 μm and channel length L_c = 80 mm	Water	Annual flow, wavy flow and dispersed flow were not observed. A droplet condensation heat transfer model was established
Garimella et al. [11]	Circular channels with 500 μm < d_p < 4910 μm	R134a	A comprehensive pressure drop model was proposed. Overlap and transition regions between respective regimes were addressed
Wu and Cheng [12]	Trapezoidal silicon parallel channels with d_p = 82.8 μm and L_c = 30 mm	Water	Vapor injection flow and its induced condensation instabilities in microchannels are reported
Zhang et al. [13]	Rectangle silicon triple-channel with aspect ratio = 27 d_p = 58 μm, L_c = 5 mm	Water	Two miniature bubble generation modes were observed: single vapor thread breakup mode and dual vapor threads breakup mode
Zhang et al. [14]	Rectangle silicon single channel with aspect ratio = 27 d_p = 58 μm, L_c = 5 mm	Water	Bubble shape, size and frequency can be controlled by cooling rate during condensation
Agarwal and Garimella [15]	Circular and noncircular channels with 424 μm < d_p < 839 μm	R134a	A model was proposed to predict condensation pressure drops in circular and noncircular microchannels. Effect of tube shape on pressure drop is demonstrated
Nebuloni and Thome [16]	Circular, elliptical, flattened, flower shaped single channel with d_p = 10 μm to 3 mm, L_c = 40 mm	R134a, ammonia	Geometrical shape in conjunction with capillary enhances overall thermal performance
Kim and Mudawar [17]	Square copper parallel channels with d_p = 1000 μm and L_c = 300 mm	FC-72	Notable heat transfer enhancement was observed for annular flow regions of micro-channel associated with interfacial waves
Ma et al. (2013) [18]	Trapezoidal silicon parallel channels with d_p = 139 μm, aspect ratio = 6.7, L_c = 50 mm	Water	Effect of non-condensable gas on condensation was investigated
Derby et al. [19]	Rectangular copper/teflon patterned parallel channels with d_p = 1060 μm, aspect ratio = 17.1, L_c = 145 mm	Water	Dropwise condensation occurs on hydrophobic teflon coated copper surfaces. High heat transfer coefficients were observed
Zhong et al. [20]	Parallel aluminum channels with fins, d_p = 1000 μm, L_c = 650 mm	R134a	Phase separation microchannel condenser (LSMC) was compared with microchannel condenser (PFMC). Better performance of LSMC was reached
Achkar et al. [21]	Single square channel with d_p = 553 μm, L_c = 196 mm	n-pentane	Three flow zones were identified: annular zone, intermittent zone, and spherical bubbles zone. Relationships were found between mean displacement and condensation velocities of elongated bubbles and their length
Mghari and Louahlia-Gualous [22]	Single rectangle silicon microchannel with d_p = 305 μm, L_c = 225 mm, aspect ratio = 0.97	Water	Liquid film thickness is calculated including effects of capillary number, Boiling number, contact angle, heat flux, vapor pressure, and hydraulic diameter

ness [22]. In the downstream part of a condenser, vapor mass qualities are reduced to induce periodic plug flow or bubbly flow [9,11,12,15,21]. Flow instability may accompany such periodic flow pattern [12]. Condensation heat transfer can be enhanced by maintaining higher vapor mass qualities [20].

The phase separation technique is also used for boiling heat transfer enhancement. Dai et al. [23] investigated single and two-phase transport phenomena using flow separation in a microgap with copper woven mesh coatings. Kandlikar [24,25] studied enhanced macro-convection mechanism with separate liquid–vapor pathways to improve pool boiling performance, and enhanced boiling heat transfer by evaporation momentum force. Jaikumar and Kandlikar [26,27] investigated enhanced pool boiling with open microchannels and feeder microchannels.

This paper is organized as follows. Section 2 describes test section and experimental setup. Section 3 describes results and discussion, including Section 3.1 for water suction towards pin fin structure, Section 3.2 for reduced pressure drops in micro condensers, Section 3.3 for heat transfer performance of PPS and SWM condensers, Section 3.4 for heat transfer performance of three micro condensers and Section 3.5 for comments on microscale phase separation condensers. Conclusions are summarized in Section 4.

2. Test section and experimental setup

2.1. The three micro-condensers

Three micro-condensers were fabricated by Microelectricalmechanicalsystem (MEMS) technique. Fig. 1 shows the solid wall microchannel condenser (SWM condenser), noting that the glass cover was not shown in Fig. 1. The silicon chip had an overall size of 37 mm × 8 mm × 0.9 mm including a glass cover. There are 31 parallel microchannels. Each microchannel had a length of 25,000 μm, a width of 78 μm and a height of 75 μm, with a fin width of 22 μm. An inlet fluid plenum was arranged to distribute vapor to each microchannel. An outlet fluid plenum collected condensed liquid from different microchannels. Two orifices were in the inlet fluid plenum and outlet fluid plenum, respectively. Each conical orifice had a minimum cross section of 1.0 mm × 1.0 mm. All the etched structure had a depth of 75 μm, which was measured by the Surface Profiler (AS500 type) with the measurement uncertainty of 25 Å. Contact angle between water and etched silicon surface was measured to be 66.8°, behaving hydrophilic nature.

Fig. 2 shows the parallel phase separation condenser (PPS condenser). The overall size and etched depth are identical to those shown in Fig. 1. Solid wall fins shown in Fig. 1 are replaced by pin-fin structure. Connection lines linking independent pin fins are parallel with each other to form periodic liquid passage and vapor passage. Each liquid passage and vapor passage had the width of 79 μm and 121 μm, respectively. Each pin fin had a planar size of 15 μm × 15 μm. The throat between neighboring pin fins had a 5 μm gap. Each liquid passage had an inlet pin fin barrier perpendicular to the axial flow direction, but outlet of the liquid passage was open to discharge liquid. The total number of liquid and vapor passages is the same as the number of microchannels shown in Fig. 1.

In order to adapt varied flow rates of vapor and liquid phases along the flow direction, PPS condenser (see Fig. 2) is modified to yield conical phase separation condenser (CPS condenser shown in Fig. 3). Along the flow direction, liquid passages are divergent
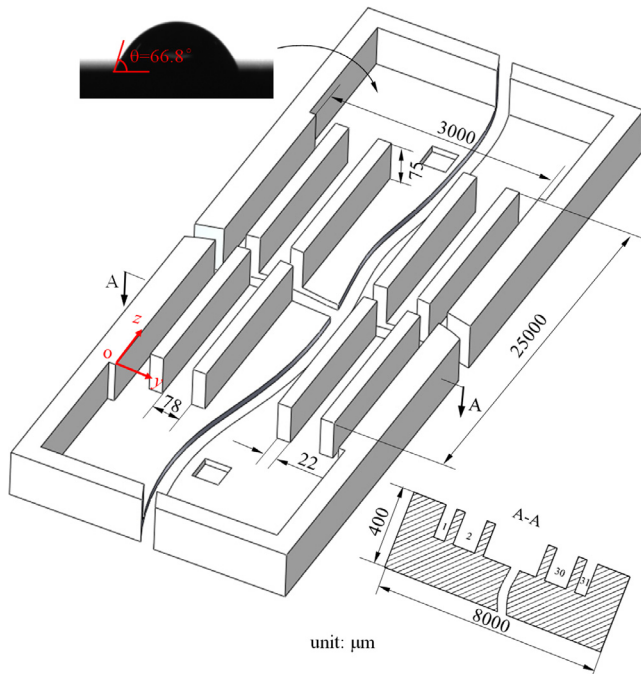
Fig. 1. Solid wall microchannel condenser (SWM: a coordinate system was established with y as the chip width direction and z as the axial flow direction, all dimensions are in μm.)

because liquid flow rates are increased, but vapor passages are convergent because vapor flow rates are decreased. For each liquid passage, the angle between two connection lines linking independent pin fins was 0.246°, yielding an inlet width of 27 μm and an outlet width of 130 μm. Alternatively, a vapor passage had an inlet width of 173 μm and an outlet width of 70 μm. Each pin fin had identical size to that shown in Fig. 2.

Fabrication of micro-condensers was as follows: (1) preparation of three silicon wafers with each having a 400 μm thickness; (2) deposition of a 2000 Å thickness SiO_2 film on the positive side of the silicon wafer by Low Pressure Chemical Vapor Deposition (LPCVD) method; (3) deposition of 1000 Å thickness Si_3N_4 films on both sides of the silicon wafer, acting as the protection and electric insulation layer; (4) selective reactive ion etching (RIE) applied on the back side of the silicon wafer to form conical shape inlet and outlet orifices with a depth of 325 μm; (5) on the positive side, KOH etching of the inlet and outlet fluid plenums with a depth of 75 μm; (6) RIE etching of the deposited Si_3N_4 and SiO_2 films; (7) deposition of aluminum film with a thickness of 1000 Å on the positive side of the silicon wafer; (8) photoresist and lithographic applied to the positive side of the silicon wafer to form the initial micro-pin-fin pattern, and wet etching applied to remove the aluminum film in the micro structure regions; (9) ASE (advanced silicon etching) of the micro structure with a depth of 75 μm; (10) etching the left aluminum film and rinsing; and (11) bonding the etched silicon chip with a 7740 glass cover.

2.2. The micro-condenser package

Fig. 4 shows micro-condenser package, consisting of a top 7740 glass cover (1) bonded with a silicon chip (2), a teflon insulation block (5), a copper block (8) and a bottom copper plate (11). The silicon chip can be SWM condenser, PPS condenser or CPS condenser. All the components are packaged with each other by four screws. The copper block was tightly embedded in the teflon insulation block. An entrance hole (3) and an exit hole (10) were
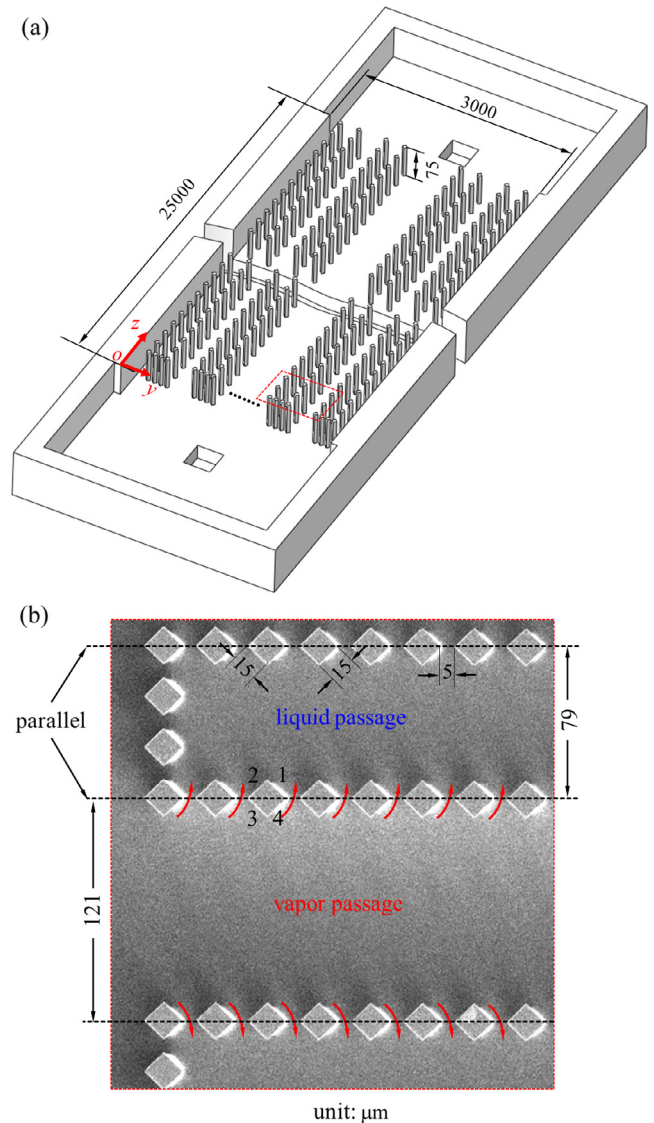
Fig. 2. Parallel phase separation condenser (PPS, a: 3D drawing of the condenser, b: entrance region).

arranged in the teflon block to penetrate inlet and outlet capillary tubes for fluid transfer. There are eleven thermocouple holes with 1.0 mm diameter to penetrate jacket thermocouples, two for fluid temperature measurements (4 and 6), and others for temperature measurements of the copper block. During the micro-condenser operation, cooling water was flowing in the channel of the bottom copper plate to dissipate heat from the silicon chip. Fig. 4b shows the copper block with a planar size of 25.0 mm by 3.0 mm, which is identical to that of the condensation region shown in Figs. 1–3. The copper block tightly contacted the bottom surface of the silicon chip with high thermal conductivity glue filled between them to decrease interfacial thermal resistance. There are three independent regions separated by miniature slots in the copper block with each slot gap of 0.8 mm. Each region had a specific heat flux q which is determined by three thermocouples arranged in the height direction. For example, for the first region, $q_1 = k \cdot \frac{dT}{dx}$, where k is the copper thermal conductivity, $\frac{dT}{dx}$ is the temperature gradient in the height x direction based on the linear correlation of T_{11}, T_{21} and T_{31}. Similarly, q_2 and q_3 were processed for the second region and third region, respectively. Each jacket thermocouple was tightly inserted in the corresponding hole with the help of the high
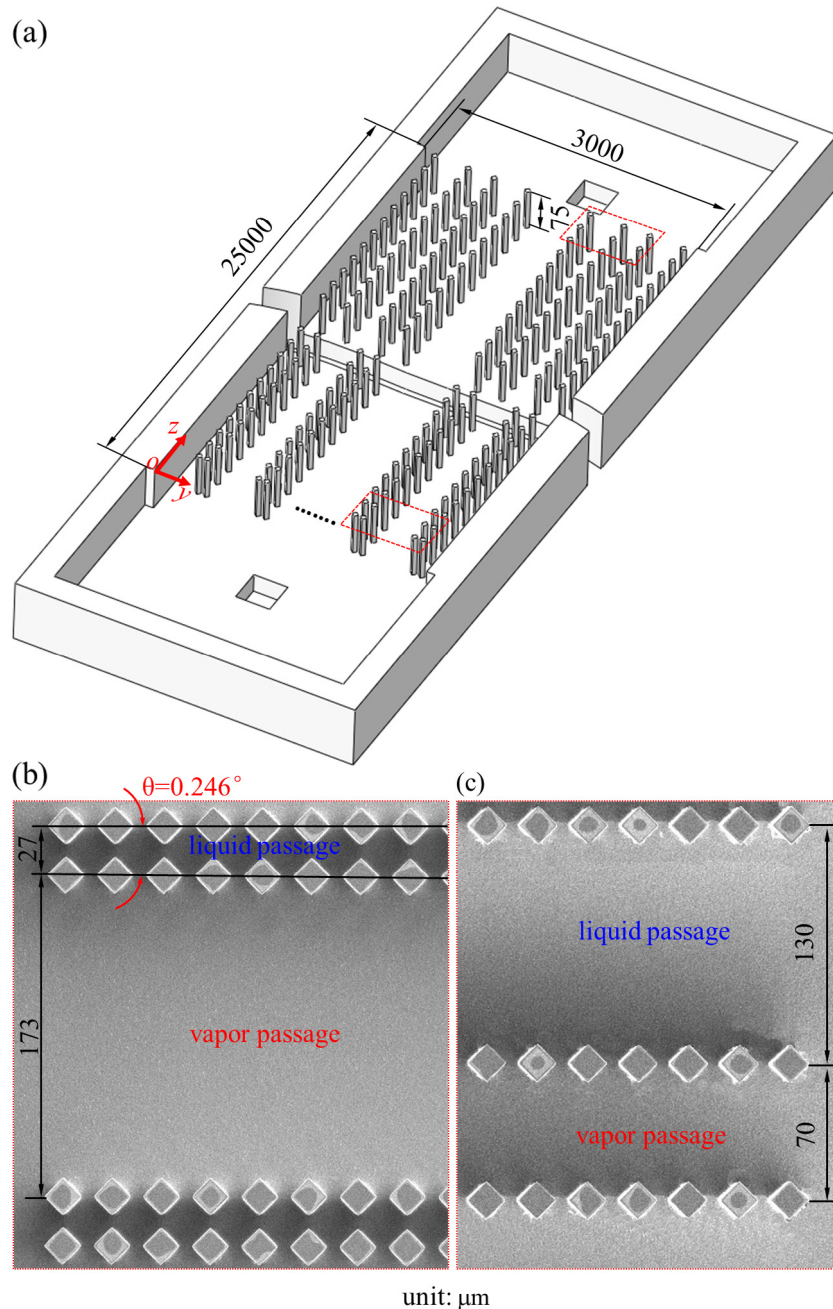
Fig. 3. Conical phase separation condenser (CPS, a: 3D drawing of the condenser, b: entrance region, c: exit region).

thermal conductivity glue. The distance between neighboring layers of thermocouples was 5.0 mm shown in Fig. 4b.

Because micro-structures are different, suitable criteria should be developed for comparative comparisons. For the three condensers, the etched depths are the same. The total number of microchannels or passages is also the same. The exposed surface area (S_2), vacuum volume not occupied by solid structure (V) and surface to volume ratio (S_2/V) were examined. Table 2 shows the three parameters. S_2 is the same for CPS and PPS condensers, but slightly larger than that for SWM condenser. However, the surface to volume ratio is almost identical for the three condensers. In other words, Figs. 1–3 are designed so that they have the same surface to volume ratio in the major condensing region. In summary, the flow and heat transfer data were presented based on the same surface to volume ratio for the three condensers.

2.3. The forced convection loop for condensation experiment

Fig. 5 shows the forced convection loop, including a pressure and temperature controlled steam boiler, a micro condenser package, a microscope bonded with a high speed camera, a post-condenser and an electronic balance for flow rate measurement of condensed water. Capillary stainless steel tube connected all components in the forced convection loop. Along the flow path of the loop, a 3 µm filter, a pressure transducer (P_{in}), a differential pressure transducer (ΔP) and two miniature thermocouples (T_{in} and T_{out}) were installed consecutively. Because the condensed water was directly discharged to a beaker at environment pressure and pressure drop downstream of the micro-condenser is significantly small, P_{in} (superficial pressure, not absolute pressure) is very close to pressure drop across the micro-condenser (ΔP). Vapor
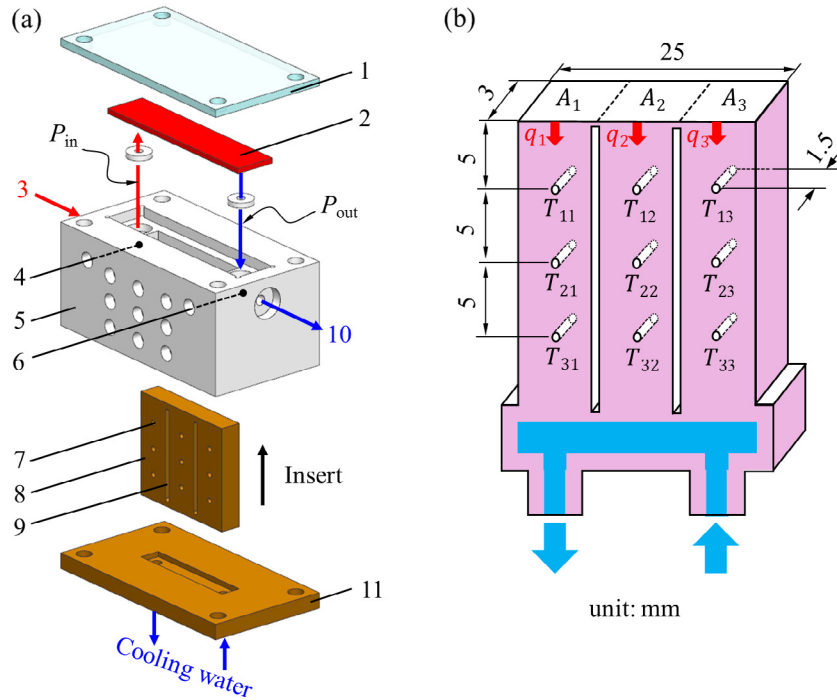
Fig. 4. Micro-condenser package (1: 7740 glass cover, 2: micro-condenser chip, 3: vapor inlet line, 4: thermocouple for vapor inlet, 5: teflon block for thermal insulation, 6: outlet fluid thermocouple, 7: thermocouple hole, 8: copper block, 9: thermal insulation slot, 10: outlet fluid line, 11: bottom copper plate).

Table 2
Parameters characterizing flow and heat transfer performance of the three condensers.

Micro-condenser	S_1 (μm²)	S_2 (μm²)	V (μm³)	S_2/V (μm⁻¹)
CPS	6.88E+07	1.92E+08	5.16E+09	0.0373
PPS	6.88E+07	1.93E+08	5.16E+09	0.0373
SWM	5.92E+07	1.67E+08	4.44E+09	0.0377

Note: S_1 is the bottom surface area excluding solid fin walls for SWM and pin fins for CPS and PPS, S_2 is the exposed surface area excluding top surface area of pin fins, V is the vacuum volume not occupied by solid structure, and S_2/V is the ratio of exposed surface area to vacuum volume not occupied by solid structure. All these parameters are defined in condensing region with the length of 25.0 mm and width of 3.0 mm (see Figs. 1–3).

temperature at the condenser inlet was measured by a K-type thermocouple located as close to the condenser as possible. Carefully designed miniature adapters connected capillary tube and micro condenser. In order to prevent vapor from condensing before entering the condenser, a small diameter metallic wire was wrapped on the capillary tube for heat compensation. The metallic wire was heated by an adjustable AC power supply. For each running case, a suitable heating power applied on the metallic wire was selected so that there was no any droplet observed at the condenser inlet. The heat compensation method ensures quasi-saturation vapor at the micro condenser entrance. The quasi-saturation vapor was ensured by examining the match of inlet vapor temperature T_{in} and saturation temperature corresponding
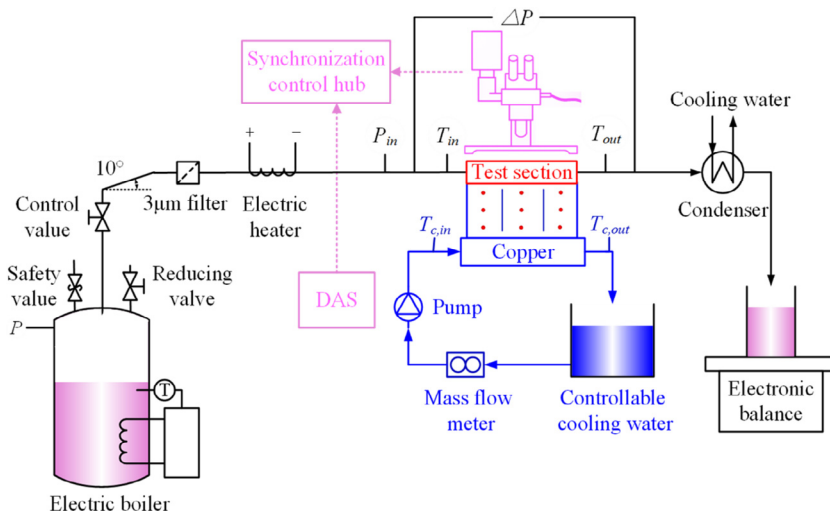
Fig. 5. Experimental setup.

to inlet pressure. For example, at a measured vapor pressure of P_{in} = 74.96 kPa, the inlet vapor temperature T_{in} was measured to be 116.8 °C, which was 0.5 °C higher than the saturation temperature of 116.3 °C corresponding to P_{in}.

For condensation experiment, it is important to remove non-condensable gas in the fluid. Initially, the whole loop was vacuumed to remove non-condensable gas. Degassed and deionized water was charged into the steam boiler. Before formal experiment, heating the water increased pressures in the steam boiler. A high precision pressure transducer and a safety valve were installed at the top of the steam boiler. The safety valve was set at a desired pressure such as about 3 bar. When the pressure reached the desired value, the safety valve automatically discharged vapor to environment. The discharging process was stopped until the vapor pressure perfectly matched its saturation temperature. A post-condenser was arranged downstream of the condenser, ensuring the two-phase mixture completely condensed to water. The condensed water was collected by a beaker which was put on an electronic balance with an uncertainty of 0.02 g.

A cooling water loop dissipated heat from micro condenser. The cooling water was circulated by a gear pump from a controlled temperature water tank. Mass flow rate, inlet temperature entering the copper plate and outlet temperature leaving the copper plate were measured.

Before condensation experiment, thermal balance between silicon chip and cooling water was examined. Calibration experiment was performed using hot water (not vapor) to flush the silicon chip. Inlet water temperature entering the silicon chip was in the range of 71.3–82.8 °C. The cooling water loop was running to dissipate heat from the silicon chip. Thermal efficiency η was defined as the heat transfer rate based on inlet and outlet cooling water temperatures divided by that based on inlet and outlet temperatures of the silicon chip. In this study, average value of η reached about 0.94, indicating the acceptable performance of the whole experimental setup. The measured data of η for different runs can be seen in Supplementary Material.

2.4. Instrumentation, measurements and uncertainties

The instruments, ranges and uncertainties of various parameters are shown in Table 3. The flow length was divided into three independent sections (see Fig. 4b). The determination of heat flux for each section q_i was described in Section 2.2. Condensation heat transfer coefficient h_i was determined using the following equation:

$$h_i = \frac{q_i}{T_{w,i} - T_{sat,i}} \tag{1}$$

where i is the section number (i = 1, 2 or 3), $T_{w,i}$ is the wall temperature at the top surface of the copper block such as A_1, A_2 or A_3

shown in Fig. 4b. $T_{w,i}$ is decided based on the linear extension of the three measured temperatures in the height direction to the top surface location. $T_{sat,i}$ is the saturation temperature at each section center, which is decided based on the assumed linear pressure distribution from condenser inlet to outlet. Eq. (1) computed condensation heat transfer coefficients assuming negligible thermal conduction resistance of silicon substrate and interfacial thermal resistance between silicon chip and copper block. The condensation heat transfer coefficient is $\sim10^4$ W/m^2 K. Considering the silicon thermal conductivity of $\sim10^2$/W/m K and the silicon chip thickness of 10^{-4} m, the thermal resistance of silicon thermal conduction is two magnitudes smaller than the thermal resistance of condensation heat transfer. Thus, the silicon chip has uniform temperature in the chip thickness direction.

Mass flux G is defined as $G = m/A_c$, where m is the mass flow rate determined by the time dependent weight measurement of condensed water. A_c is the summed cross sectional area of all microchannels for SWM condenser. For PPS or CPS condenser, A_c is decided as $A_c = W_n H_e$, where W_n is the total width at the narrowed location along the flow direction, and H_e is the etched depth of 75 μm. It is noted that for CPS condenser, both $A_{c,l}$ for liquid passage and $A_{c,v}$ for vapor passage are changed along the flow direction, but the sum of them equals to A_c and is constant along the flow direction.

Pressures, temperatures and mass flow rate of cooling water were recorded by a high speed data acquisition system (DL 750, Yokogawa, Inc., Japan) with 16 channels. The data sampling rates can reach 10 million samples per second. In this study, the recording rate was selected as 100 samples per second, which is fast enough to capture the response time of these signals. A high speed camera (IDT Motion pro Y4) incorporating a stereo microscope (Nikon SMZ1500) allows for the condensation flow visualization. A synchronization control hub triggers the function of the high speed data acquisition system and the flow visualization system simultaneously, with a time uncertainty of 20 ns. The uncertainties of various parameters are summarized in Table 3.

3. Results and discussion

3.1. Water suction towards liquid passage

For PPS and CPS condenser, the lined pin fin array with a gap of 5 μm functions as the separation membrane. Before condensation experiment, water drop attraction experiment was performed to demonstrate hydrophilic characteristic of pin fin structure. Initially, the silicon chip (without glass cover) was dry (see Fig. 6a). A water drop was slowly injected from a 100 μm diameter needle (see images from 0 to 20.8 ms in Fig. 6a). During the injection process, the drop directly contacted with the bottom surface of the inlet fluid plenum, with the drop interface approaching the pin

Table 3
Instruments, ranges and uncertainties for condensation experiments.

Parameters	Explanations	Measurements	Ranges	Uncertainties or relative error
A_c	Cross section area	Determined by MEMS fabrication technique	/	0.001%
G	Mass flux in condenser based on narrowed cross sectional area	Measured by electronic balance over time	31.73–153.74 kg/m^{2}s	0.11%
h	Condensation heat transfer coefficient	Calculated by Eq. (1)	1.34×10^3–2.40×10^4 W/m^2 K	0.6–2.5%
m_c	Cooling water flow rate	Coriolis mass flow meter (DMF-1-1AB)	0.16–0.75 g/s	0.6%
P_{in}	Inlet superficial pressure of condenser	Pressure transducer (Rosemount-3051)	2.44×10^4–1.35×10^5 Pa	0.1%
ΔP	Pressure drop across condenser	Pressure transducer (Rosemount-3051)	2.73×10^4–1.37×10^5 Pa	0.1%
q	Heat flux	Determined by temperature measurements	124.65–753.93 kW/m^2	0.3–1.3%
T_{in}, T_{out}	Inlet and outlet temperature of working fluid across condenser	K-type thermocouple	32.2–124.9 °C	0.3 °C
T_{11}, T_{12}, T_{13}	Copper block temperature	K-type thermocouple	25.7–91.0 °C	0.3 °C
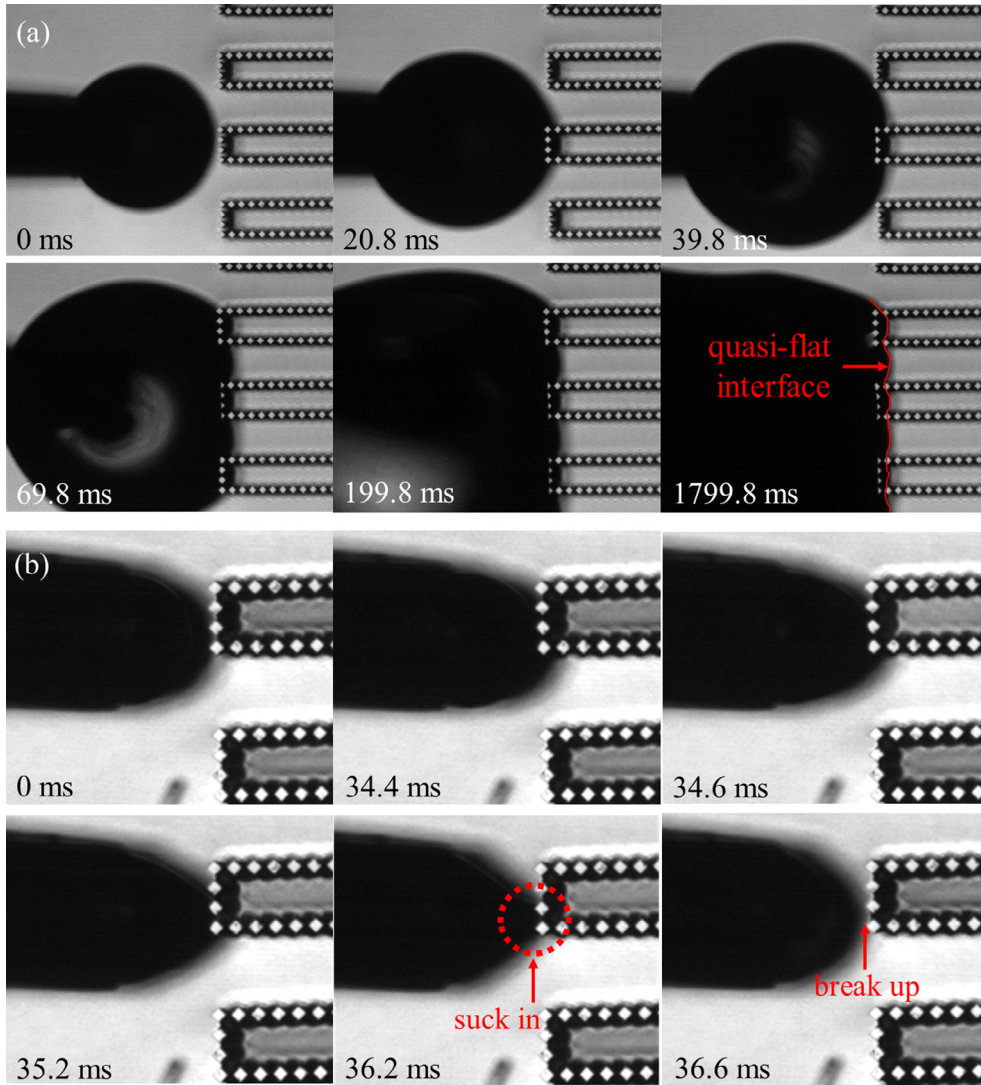
Fig. 6. Water droplet advancing pin fin structure (a: droplet advancing dry pin fin with quasi-flat ending interface, b: quick suction of water thread towards wet pin fin structure, the droplet was receding from pin fin after breakup of the suction thread.)

fin membrane in the period of 20.8–199.8 ms. The drop interface was finally stopped near the vertically lined pin fin membrane and did not enter the pin fin envelope anymore.

Fig. 6b shows different situation. Initially, inside the pin fin envelope was wet, but outside the pin fin envelope was dry. A water drop was slowly being injected from the pin fin outside. When the water drop interface approached the pin fin membrane, a thin water thread was quickly formed and sucked towards the pin fin envelope. Because the pin fin membrane generates apparent attracting force, the water thread was instantaneously broken up. Thus, the bulk drop receded from the pin fin membrane.

Fig. 7a shows the drop interface approaching dry pin fins. Fig. 7b shows the photo with the finally stabilized gas-liquid interface. Two neighboring pin fins were considered as a system. Gibbs free energy was analyzed to explain the interface advancing pin fin throat location. The gas-liquid interface was initially at $t = t_1$, with the curvature center point marked as O. The interface travels a distance of l_1 measured on pin fin side wall to be at $t = t_2$, with the curvature center point marked as O'. The parameter l_1 is also called the wetting length. Contact angle is $\theta = 66.8°$ between water and silicon material. Gibbs free energy G_{Gibbs} is written as

$$G_{Gibbs} = \gamma_{sg}A_{sg} + \gamma_{sl}A_{sl} + \gamma_{lg}A_{lg} \tag{2}$$

where γ is the surface tension, A is the interface area, the subscripts s, g and l represent solid, gas and liquid, respectively. For the problem studied in Fig. 7a, another parameter is introduced as $G_{Gibbs,c} = \gamma_{sg}A_t$, where A_t is the total side wall area of pin fins. With the help of Young's equation, Eq. (2) becomes

$$G_{Gibbs} = G_{Gibbs,c} + (A_{lg} - A_{sl}\cos\theta)\gamma_{lg} \tag{3}$$

At $t = t_2$, the following expressions exist:

$$A_{lg} = 2\alpha r_1 H_e \tag{4}$$

$$A_{sl} = 2l_1 H_e \tag{5}$$

where α is the angle shown in Fig. 7a, r1 is the radius from O' to A, H_e is the fin height of 75 μm. The following equation exists by applying the law of sines to the triangle AOO'.

$$\frac{r_1}{\sin\angle AOO'} = \frac{L - l_1}{\sin(\pi - \alpha)} \tag{6}$$

where L is the curvature radius at the initial location at t_1. Substituting $\angle AOO' = \pi/4$, $\alpha = 3\pi/4 - \theta$, $\theta = 66.8°$ and $L = 18.54$ μm into Eq. (3) yields

$$r_1 = 15.05 - 0.78l_1 \tag{7}$$
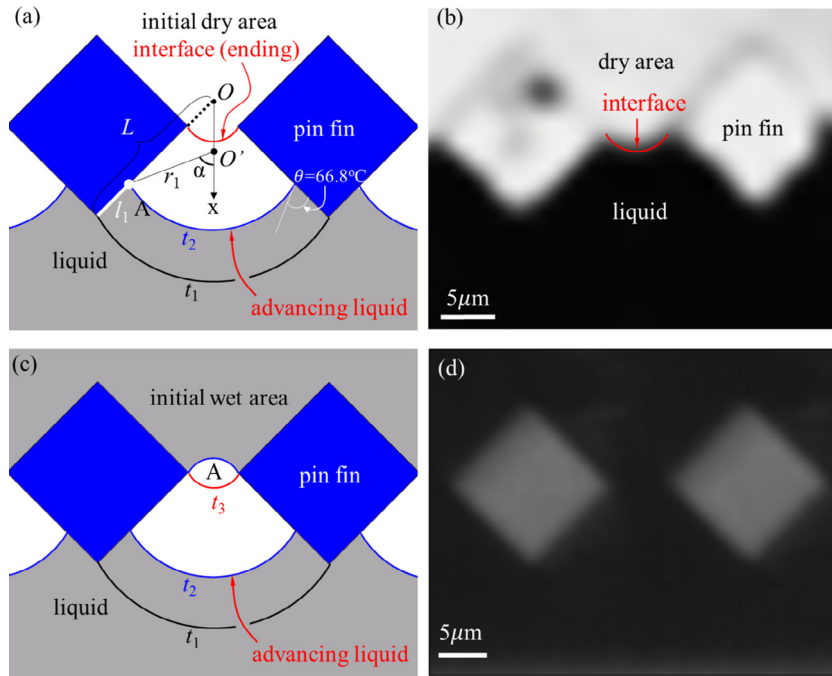
Fig. 7. Gas–liquid interface advancing pin fin throat (a: back side is initially dry, b: photo showing the finally stabilized interface, c: back side is initially wet, d: photo showing liquid coalescence from both sides of pin fins).

It is noted that both r_1 and l_1 have the unit of micron. Finally, the Gibbs free energy is

$$G_{Gibbs} = G_{Gibbs,c} + (34.04 - 2.44l_1)H_e\gamma_{lg} \qquad (8)$$

Differentiating G_{Gibbs} with respect to l_1 yields

$$\frac{\partial G_{Gibbs}}{\partial l_1} = -2.44 H_e \gamma_{lg} < 0 \qquad (9)$$

Eq. (9) indicates decreased Gibbs free energy with the gas-liquid interface approaching throat location of pin fins. The interface finally stops at the throat location, marked by the red curvature shown in Fig. 7a and b. If the back side of pin fin membrane is wet, gas-liquid interface advancing from the front side yields liquid coalescence of both sides (see Fig. 7c and d). Duration the operation of PPS or CPS condensers, liquid passages are occupied by liquid. Condensed liquid in vapor passages can be sucked towards liquid passage due to the decreased Gibbs free energy, accounting for the phase separation mechanism. Practically, vapor passages contain annular flow pattern having vapor core with liquid film on solid walls. The lined pin fin array attracts liquid film towards liquid passage. Thus, in vapor passages, liquid film thickness is decreased to account for the enhanced condensation heat transfer. Similarly, Michielsen et al. [28] performed the Gibbs free energy analysis to determine the movement of a drop along a cone fiber. In summary, the decreased Gibbs free energy with gas-liquid interface advancing pin fin throat accounts for the phase separation mechanism. Both our analysis and experiments show that vapor never enters the liquid passage, because a larger capillary pressure should be overcome if that situation occurs.

3.2. Reduced pressure drops for phase separation condensers

For any micro-condenser, a running case was specified by setting a given upstream pressure of micro-condenser P_{in} (P_{in} almost equals to pressure drop ΔP across condenser) and a cooling water flow rate (m_c). Mass fluxes are increased by raising inlet pressures, or say pressure drops, see Fig. 8a–c. In order to identify the phase

separation effect on pressure drops across condensers, G_{PPS}/G_{SWM}, the ratio of mass flux of PPS condenser with constant cross section area to that of SWM condenser, was plotted in Fig. 8d. G_{PPS}/G_{SWM} is larger than 1.0 at $m_c = 0.167$ g/s and 0.472 g/s, indicating that PPS condenser decreased pressure drops at moderate or smaller cooling water flow rates. But G_{PPS}/G_{SWM} is less than 1.0 at $m_c = 0.750$ g/s. Later it will be shown that increased pressure drops of PPS condenser is caused by over liquid expansion at larger cooling intensities. Fig. 8e shows decreased pressure drops by CPS condenser. At the same pressure drop, PPS or CPS condensers increase mass fluxes by about 15%, maximally.

Parmar and Majumder proposed a model to describe hydrodynamics of microbubble suspension flow in pipes [29]. They assumed that pressure drop in pipes is related to energy dissipation between two-phases of liquid and microbubbles, and between two-phase mixture and pipe wall. Here, such model was extended to explain the phase separation effect on pressure drops. A channel contains two-phase mixture of vapor and liquid droplets. No heat and mass transfer happen in the system. The following equation exists

$$\Delta P A_p v_m - E = 0 \qquad (10)$$

where A_p is the channel cross sectional area, v_m is the velocity of two-phase mixture. E is the energy dissipation, containing two components: energy dissipation due to interaction between vapor and liquid droplet per unit volume of the two-phase mixture, E_{lg}, and energy dissipation due to interaction between two-phase mixture and channel wall, $E_{tp,w}$. That is $E = E_{lg} + E_{tp,w}$. E_{lg} is dealt with first. For a single droplet with a diameter of d_d, the frictional force between vapor and droplet is

$$F_d = C_d A_s \frac{1}{2}\rho_g v_s^2 = \frac{1}{8}\pi d_d^2 C_d \rho_g v_s^2 \qquad (11)$$

where A_s is the projected surface area of the droplet, C_d is the drag coefficient of a droplet in a flowing vapor, ρ_g is the vapor density, v_s is the slip velocity between liquid and vapor: $v_s = v_g - v_l$, v_g is the vapor velocity and v_l is the droplet velocity. Energy dissipation
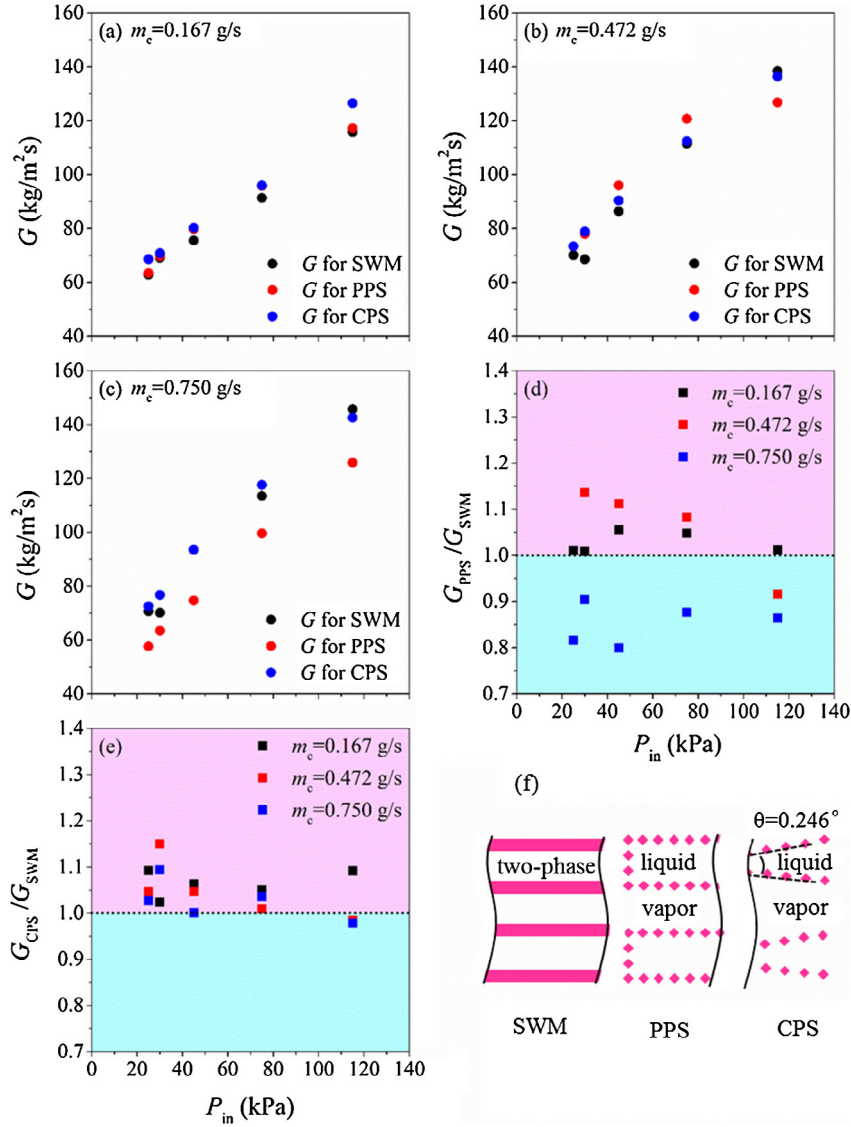
Fig. 8. Mass fluxes versus inlet pressures (or say pressure drops) for the three micro-condensers.

due to interfacial interaction between two-phases is the sum of all droplets in the system:

$$E_{lg} = F_d v_l N_d = \frac{1}{8}\pi d_d^2 C_d \rho_g v_s^2 v_l N_d \tag{12}$$

where N_d is the number of droplets, which can be computed as [29]

$$N_d = \frac{6(1-\beta)A_p L_c}{\pi d_d^3} \tag{13}$$

where L_c is the channel length, β is the volume ratio of the vapor phase to the two-phase mixture, which is [29]

$$a = \frac{6(1-\beta)}{d_d} \tag{14}$$

Thus, E_{lg} is rewritten as

$$E_{lg} = \frac{1}{8}C_d \rho_g v_s^2 v_l A_p L_c a \tag{15}$$

C_d is related to droplet Reynolds number Re which is in low or moderate region. C_d is increased with decrease of droplet diameter d_d [30]. Eq. (15) tells us that energy dissipation between vapor and droplets is increased for small droplets, due to the increased drag

coefficient C_d and interfacial area a when the size of droplets is decreased. $E_{tp,w}$ is

$$E_{tp,w} = F_{tp,w} v_m = \tau_{tp,w}\pi d_p L_c v_m \tag{16}$$

where $\tau_{tp,w}$ is the shear stress between two-phase mixture and channel wall, d_p is the channel diameter. Combining Eqs. (10), (15) and (16), the pressure drop gradient along the flow direction is

$$\frac{\Delta P}{L_c} = \frac{E_{lg} + E_{tp,w}}{v_m A_p L_c} = \frac{\frac{1}{8}C_d \rho_g v_s^2 v_l A_p a + \tau_{tp,w}\pi d_p v_m}{v_m A_p} \tag{17}$$

Because $\tau_{tp,w}$ is not sensitive to the velocity difference between the two-phases, $\tau_{tp,w}$ can be computed using the homogeneous two-phase model [31], assuming the identical velocity of the two-phases for the energy dissipation between two-phase mixture and tube wall. For the energy dissipation between the two-phases, the velocity difference between the two-phases is considered (see Eqs. (11) and (12)). Because small droplet increases drag coefficient of droplet and interfacial area between the two-phases, pressure drops are increased when droplet size is decreased. This finding explains the reduction of pressure drops in phase separation condensers. The dominant mechanism for pressure drop reduction in

PPS and CPS condensers is the decreased interfacial area to reduce the energy dissipation between the two-phases.

3.3. Heat transfer performance of PPS and SWM condensers

Heat fluxes q and condensation heat transfer coefficients h are plotted in Figs. 9 and 10, noting that both q and h are determined based on the plane surface area. Comparative presentations are given for PPS (red curves) and SWM (black curves) in Fig. 9. For each case, q and h are plotted at three axial locations, corresponding to three independent regions (see Fig. 4b). PPS condenser had larger heat fluxes and condensation heat transfer coefficients at $m_c = 0.472$ g/s, evidenced by the fact that red curves are above black curves (see Fig. 9a and b). PPS condenser deteriorated heat transfer compared with SWM condenser at $m_c = 0.750$ g/s (see Fig. 9c and d). Fig. 10 plots heat flux ratio of PPS condenser with respect to SWM condenser, q_{PPS}/q_{SWM}, and heat transfer coefficient ratio of PPS condenser with respect to SWM condenser, h_{PPS}/h_{SWM}, which are larger than 1.0 at $m_c = 0.472$ g/s. PPS condenser increased heat flux by 34% and heat transfer coefficient by 62% at $P_{in} = 30$ kPa, maximally. At $m_c = 0.750$ g/s, PPS condenser decreased heat flux by 17% and heat transfer coefficient by 25%, maximally.

The experimental findings are explained here. Microchannel fin walls (SWM condenser) function as extended heat transfer area. Condensation heat transfer depends on flow patterns. Phase separation condenser changes flow structures. For ideal working condition, liquid flows in liquid passage, while vapor is condensed in vapor passage. Liquid film beneath vapor core is attracted by pin fin structure to flow towards liquid passage. For each pin fin, two side walls facing liquid passage is immersed in pool liquid, but the two side walls facing vapor passage are covered by thin liquid films. Thin liquid films on bottom wall of vapor passage and pin fin side walls account for heat transfer enhancement in PPS condenser.

The above analysis is correct for vapor-liquid interface located near pin fin membrane, such as encountered in Figs. 9a and b and 10a and b, under which condensed water flow rate in PPS condenser is not large. The degree of heat transfer enhancement is decreased for larger inlet vapor pressure or cooling water flow rate (see Figs. 9c and d and 10c and d).

Fig. 11 analyzes ideal phase separation and over liquid expansion. At the exit location, pressures are recorded as $P_{e,l}$ in liquid passage and $P_{e,v}$ in vapor passage, respectively (see Fig. 11a). Fig. 11b–g compares ideal phase separation and over liquid expansion. For normal condensing, two side walls of pin fins are covered by thin liquid film to enhance heat transfer (see Fig. 11b, d and f). At the exit location of $z = z_e$, pressures are the same for vapor passage and liquid passage. Upstream of the exit location, pressure in vapor passage P_v is larger than P_l in liquid passage. This is because vapor passage contains two-phase flow with vapor core surrounded by liquid films, while liquid passage contains pure liquid flow. Pressure difference $P_v - P_l$ maintains vapor-liquid interface near pin fin membrane, making pin fins to be useful for condensing heat transfer. For over liquid expansion, condensing intensity is large to yield large condensed water flow rate in liquid passage (see Fig. 11c, e and g). Cross sectional area of liquid passage is not sufficient to keep vapor-liquid interface near pin fin membrane. In other words, liquid is expanded from liquid passage to vapor passage to adapt the increased water flow rate. The over liquid expansion expands liquid passage and narrows vapor passage. This effect not only increases vapor pressure P_v and decreases liquid pressures P_l to stabilize vapor-liquid interface somewhere away from pin fin membrane, but also increases shear stress on vapor-liquid interface to pull liquid flowing downstream. Because all the four side walls of pin fins are flooded by liquid, pin fins are not useful for condensing heat transfer. In Fig. 11e, $P_{v,i}$ and $P_{l,i}$ are vapor pressure and liquid pressure, respectively, assuming
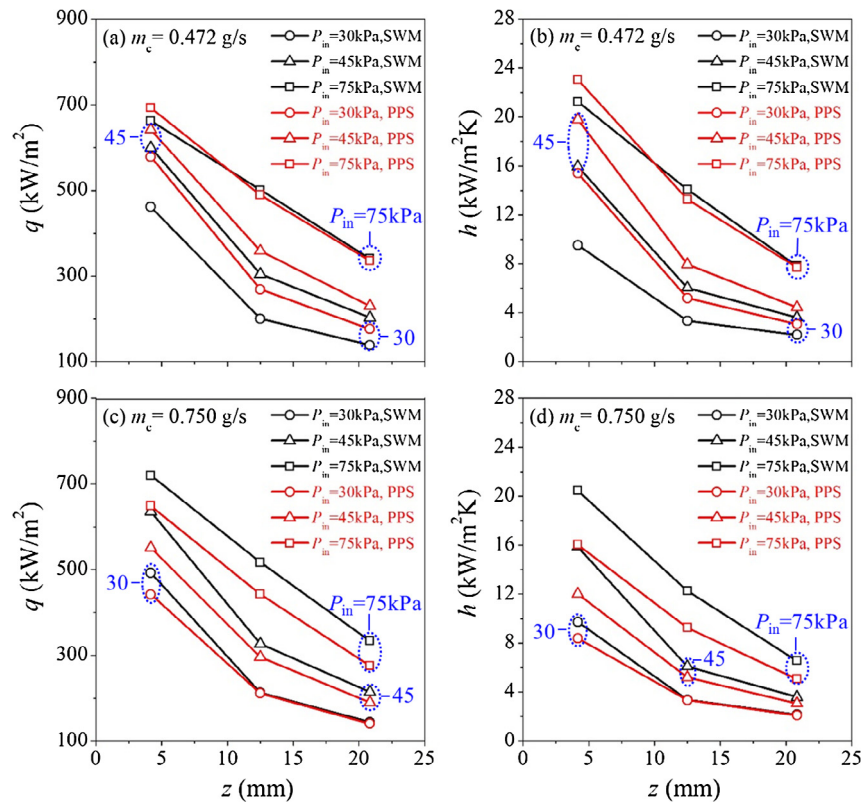
Fig. 9. Comparison of local heat fluxes and condensation heat transfer coefficients between PPS and SWM condensers.
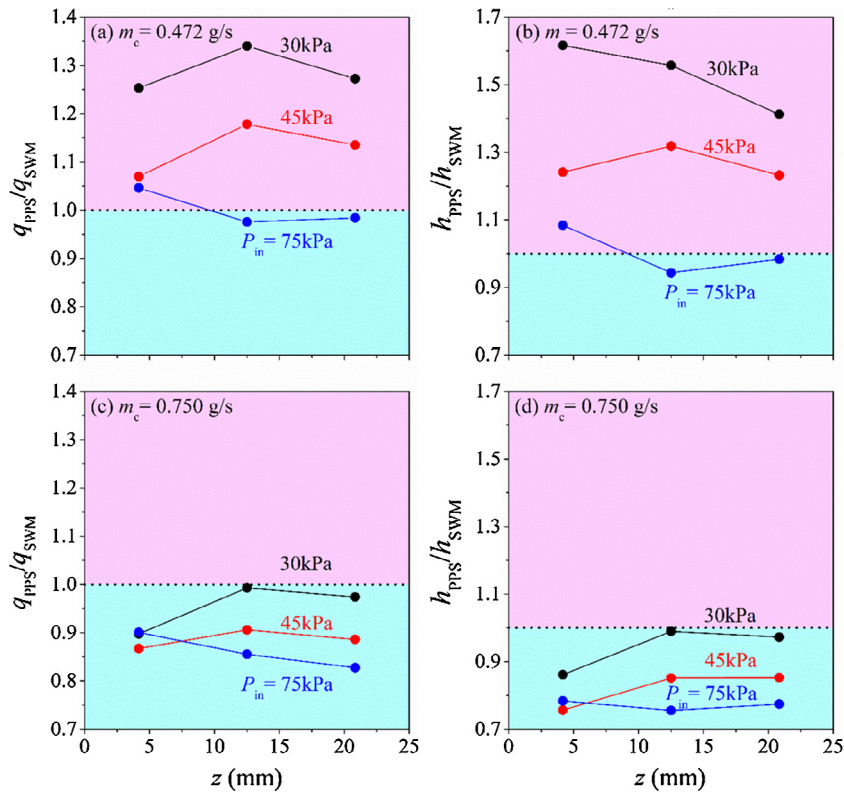
Fig. 10. q_{PPS}/q_{SWM} and h_{PPS}/h_{SWM} at two different cooling water flow rates (pink area and blue area represent the ratio values larger than 1.0 and smaller than 1.0, respectively.)

vapor-liquid interface near pin fin membrane. In fact, pressures are changed to $P_{v,a}$ and $P_{l,a}$ for vapor-liquid interface deviating from pin fin membrane due to over liquid expansion (OLE). Fig. 11f shows the direct observation of vapor-liquid interface located near pin fin membrane for moderate cooling intensity. On the contrary, Fig. 11g illustrates over liquid expansion with the vapor-liquid interface far away from pin fin membrane when cooling intensity is enhanced.

3.4. Heat transfer performance of the three condensers

CPS condenser with varied cross section areas of each fluid phase adapts variations of both liquid flow rate and vapor flow rate along the flow direction. For phase separation condenser, velocities are expressed as $v_v = m_v/(\rho_v A_{c,v})$ for vapor phase and $v_l = m_l/(\rho_l A_{c,l})$ for liquid phase, where m is the flow rate, ρ is the density, $A_{c,v} = W_v H_e$, $A_{c,l} = W_l H_e$, W_v is the width of all the vapor passages at specific axial location, W_l is the width of all the liquid passages at specific axial location. Along the flow direction, m_v is decreased but m_l is increased. CPS condenser keeps suitable slip velocity between the two phases, under which shear stress is sufficient to maintain vapor-liquid interface near pin fin membrane, so that pin fin side walls facing vapor passage are covered by thin liquid film to enhance heat transfer.

Fig. 12 shows heat fluxes and condensation heat transfer coefficients for CPS condenser compared with SWM condenser. For each group of inlet pressure P_{in} (or say pressure drop across condenser), red curves are always above black curves, indicating heat transfer enhancement of CPS condenser over the whole experimental data ranges. Fig. 13 demonstrates q_{CPS}/q_{SWM} and h_{CPS}/h_{SWM}, which are always larger than 1.0. CPS condenser increased condensation heat transfer coefficient by 74% compared with SWM condenser, maximally. By comparing Figs. 10 and 13, one observes largest condensation heat transfer coefficients for CPS

condenser and smallest condensation heat transfer coefficients for SWM condenser. An alternative way to compare the thermal performance of the three condensers is to plot q and h versus average vapor mass qualities x (see Fig. 14). The phase separation effect is significant at low or moderate vapor mass qualities. It is more useful to improve heat transfer at micro-condenser downstream.

Fig. 15 shows how CPS condenser overcomes over liquid expansion. A quarter of vapor passage is selected due to geometry symmetry, including half pin fin height and half vapor passage width. For PPS condenser, over liquid expansion narrows real vapor flow passage to flood whole pin fins and deteriorate heat transfer (see Fig. 15a). CPS condenser keeps vapor-liquid interface near pin fin structure to keep thin liquid film on two side walls of pin fins (see Fig. 15b). Fig. 15c presented $A_{c,v}$ and $A_{c,l}$. Fig. 15d shows P_v and P_l for the two condensers. For PPS condenser, assuming vapor-liquid interface still located near the pin fin structure, pressures are recorded as $P_{v,p}$ and $P_{l,p}$ to show a narrowed band. Practically, pressure difference in the chip width direction, ΔP_{PPS}, is not sufficient to maintain vapor-liquid interface near pin fin structure. Thus, over liquid expansion happens to raise the pressure difference between vapor side and liquid side. For CPS condenser, the decreased vapor passage and increased liquid passage hold sufficient pressure difference between vapor and liquid sides, ΔP_{CPS}, to keep vapor-liquid interface near pin fins. CPS condenser has self-adaptive flow passages responding to flow rate variations along the flow direction. Fig. 16 shows the phase distribution image, providing direct evidence that CPS condenser successfully overcomes the over liquid expansion effect. It is noted that flow instability was not observed in phase separation condensers, due to separated flows of vapor phase and liquid phase with quasi-stable vapor-liquid interface. Stable inlet pressures, vapor temperatures and temperatures in the copper block can be seen in Fig. S2 (see Supplementary Material).
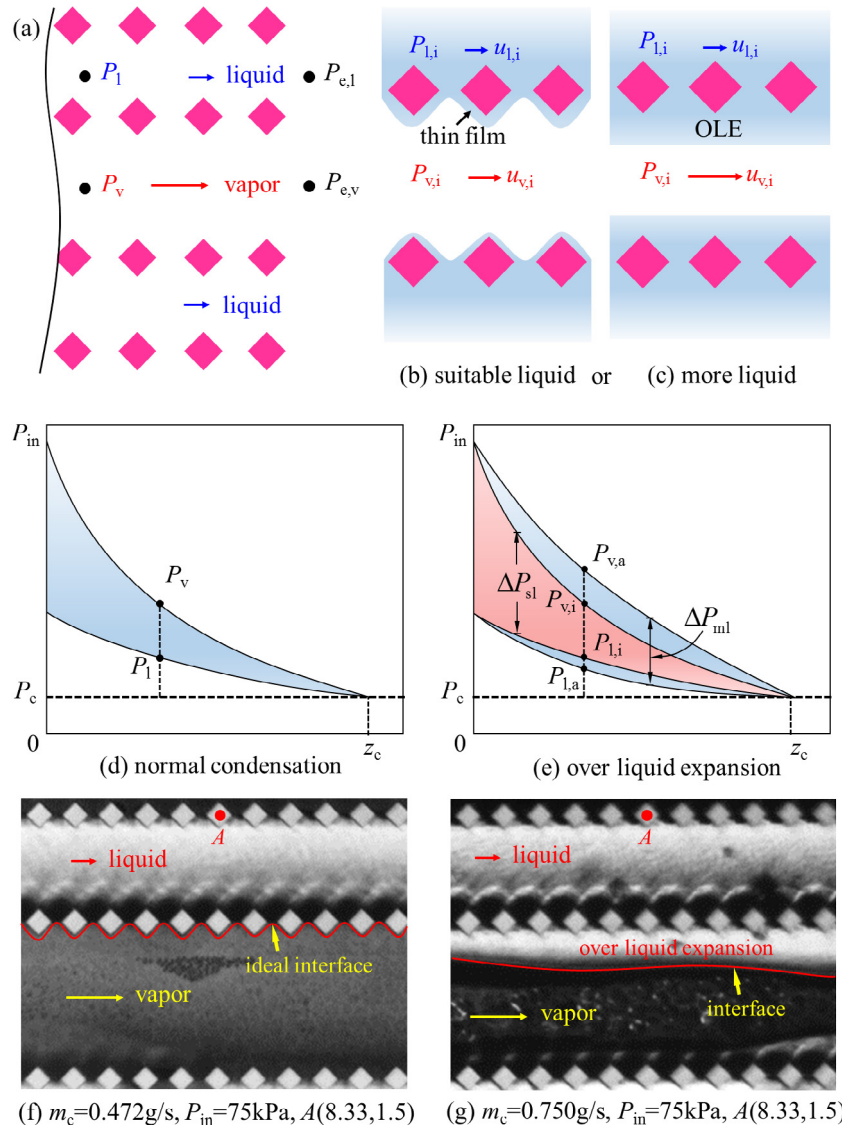
Fig. 11. Normal and abnormal condensation for PPS condenser (a: liquid and vapor passages, b: suitable liquid case, c: more liquid case, d: pressures in vapor and liquid passages for normal condensation, e: pressures in vapor and liquid passages for over liquid expansion, f: photo of the phase distribution for normal condensation, and g: photo for over liquid expansion. Point A is located at $z = 8.33$ mm and $y = 1.50$ mm.)

3.5. Comments on the phase separation condensers

From hydrodynamic point of view, phase separation condensers are helpful to reduce pressure drops to decrease pumping powers. This paper gave a general analysis about this. The phase separation technique significantly decreases interfacial area between the two-phases to minimize energy dissipation in condensing systems. From heat transfer point of view, any micro-structure should act as extended surface area to enhance heat transfer. Most heat exchangers use hydrophilic materials such as silicon, copper and stainless steel. Keeping thin liquid film on such material surface is an effective way to maintain better heat transfer performance.

Micro-condensers use pin fin structure to function vapor-liquid separation. The decreased Gibbs free energy for vapor-liquid interface advancing pin fin throat location is the mechanism to separate two-phases during continuous condensing flow along the flow direction. For phase separation condenser with constant cross sections, apparent heat transfer enhancement and pressure drop reduction are found if the cooling intensity is not too large. However, such performance is deteriorated for high cooling intensity,

or large condensed liquid flow rate in the condenser. Over liquid expansion deteriorates the performance. This finding encouraged us to invent phase separation condenser with varied cross sections. CPS condenser not only enhances heat transfer, but also reduces pressure drops, due to vapor-liquid interface successfully modulated near pin fins.

This is the preliminary work on phase separation condenser with varied cross sections. Many factors, such as condenser geometrical parameters, operating parameters and working fluid influence condenser performance. More experiment investigations, numerical simulations and condenser optimization are recommended for future work.

Recently, with the increased availability of micro/nano fabrication technologies, and new materials, there has been an increased focus on condensing in micron/nano scale, including modified surface wettability [32]. Heat transfer surfaces are often inspired by nature, such as the lotus leaf [33]. Understanding surface geometry and chemistry on droplet dynamics to improve the performance continues to be a challenge [34]. These surfaces are susceptible to contamination and long-term degradation effects, introducing
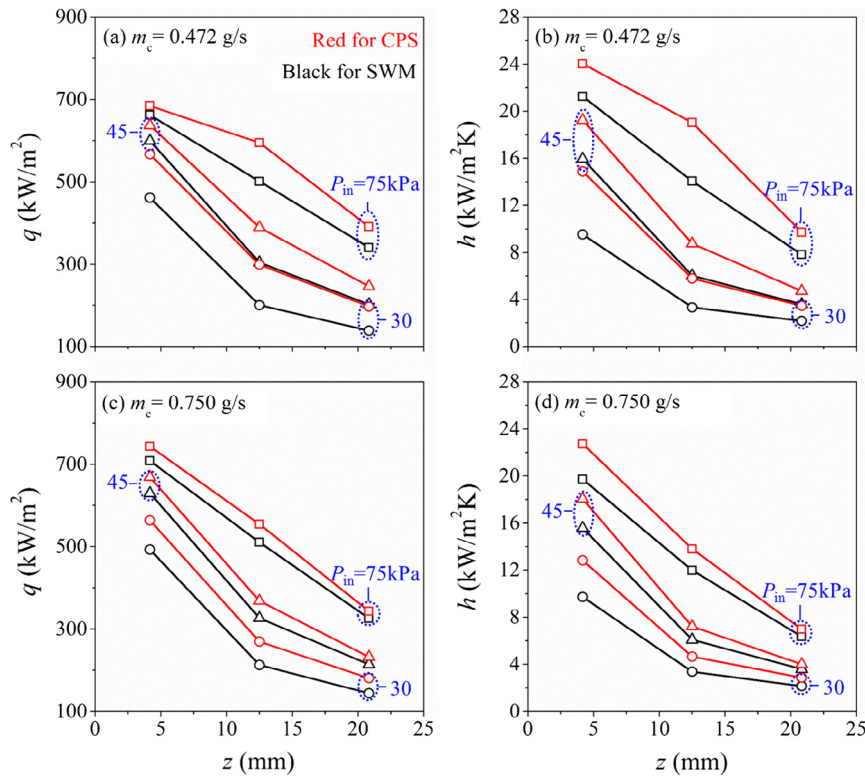
Fig. 12. Local heat fluxes and condensation heat transfer coefficients for CPS and SWM condensers.
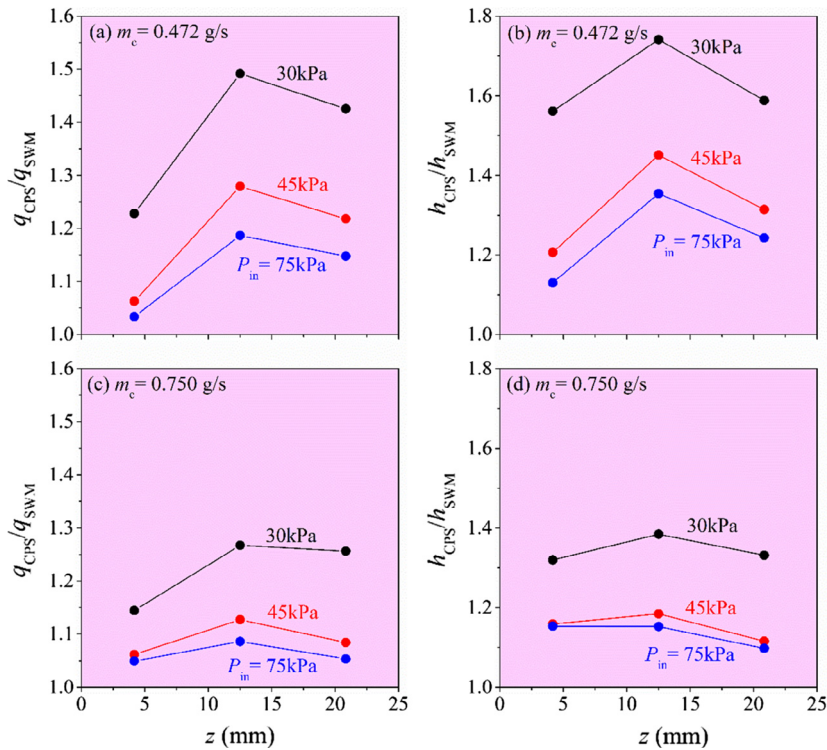
Fig. 13. q_{CPS}/q_{SWM} and h_{CPS}/h_{SWM} at two cooling water flow rates (noting that all the ratio values are larger than 1.0).

new obstacles to overcome before commercial applications [35]. The newly proposed phase separation condenser with varied cross sections needs micro-structure to fulfill phase separation. Nano structures on surfaces are not involved. Thus, the condenser can be reliable and sustain long term operation.

A prospect was made to improve plate type condenser performance using the phase separation concept. Large scale plate type condensers are widely used in energy and power engineering. These heat exchangers are compact and behave better heat transfer performance, but pressure drops are relatively larger [36]. The gap
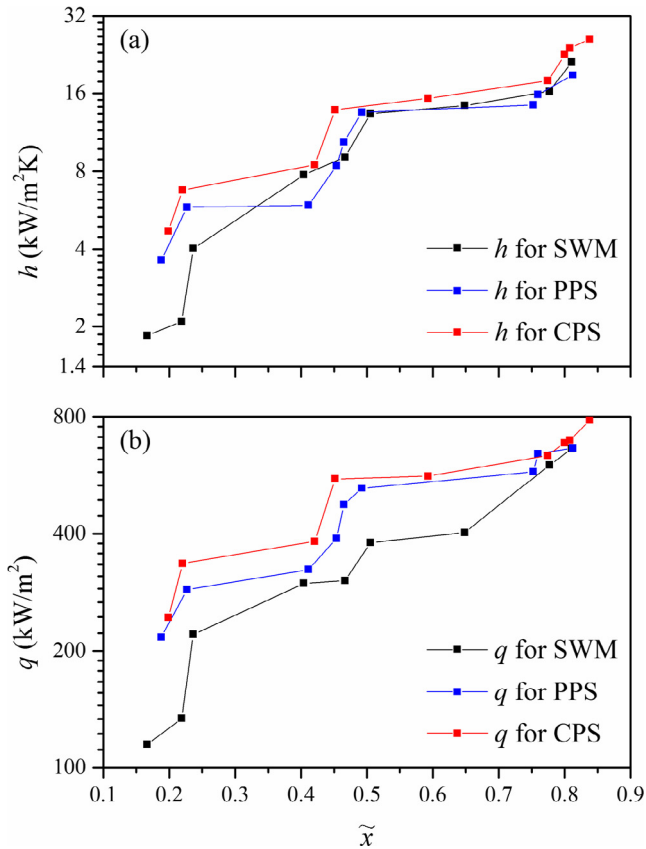
Fig. 14. Condensation heat transfer coefficients (a) and heat fluxes (b) versus vapor mass qualities.
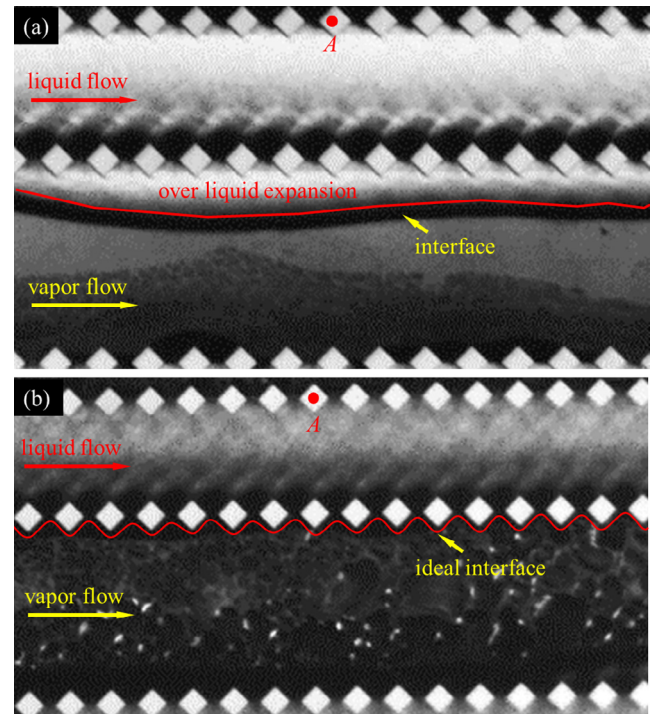
Fig. 16. Observation of over liquid expansion for PPS and ideal interface near pin fin membrane for CPS (a: P_{in} = 75 kPa, m_c = 0.472 g/s, PPS; and b: P_{in} = 75 kPa, m_c = 0.472 g/s, CPS. point A is at z = 12.50 mm and y = 1.50 mm.)
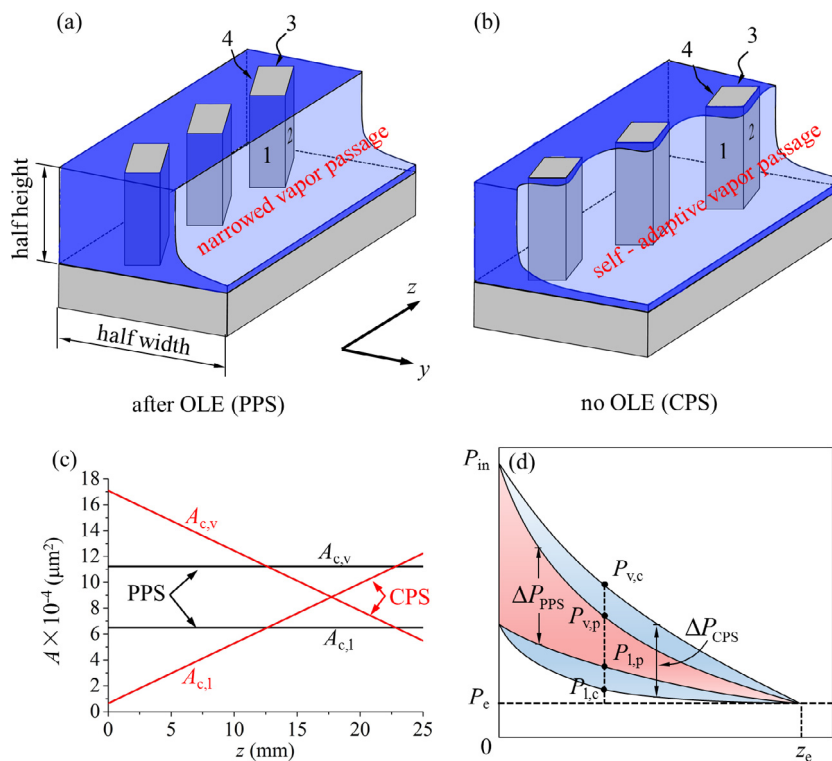
Fig. 15. Phase and pressure distribution for PPS and CPS condensers (a: pin fin side walls flooded by liquid for PPS over liquid expansion, b: two side walls of pin fin covered by thin liquid films for CPS, c: cross section areas of vapor and liquid passages for PPS and CPS, d: pressures in liquid and vapor passages for PPS and CPS).

between neighboring plates is usually in millimeter scale [36]. The mechanical engineering is able to fabricate suitable microstructures in the plate gap to separate vapor-liquid phases. Thus, the plate type condenser performance can be further improved using the phase separation concept. Especially, the decrease of pressure drops in plate type condensers is attractive for industry applications.

4. Conclusions

Three micro condensers are designed, fabricated and tested. The core concept is to use lined pin fin arrays to perform phase separation in condensers. Following conclusions are drawn:

- Gibbs free energy is analyzed for gas-liquid interface advancing throat location of pin fins. The decreased Gibbs free energy is the mechanism for pin fin membrane to capture liquid.
- An analysis is performed for energy dissipation of condensing flow in channels. Energy dissipation is increased for small droplets system. Phase separation condenser decreases interfacial area between two-phases to decrease energy dissipation, accounting for pressure drop reduction.
- PPS condenser enhances heat transfer at small or moderate cooling intensities. Heat transfer is deteriorated at large cooling intensities. Over liquid expansion occurs to flood whole pin fin side walls, deviating vapor-liquid interface from pin fin membrane.
- CPS condenser adapts variations of flow rates of the two phases along the flow direction. Over liquid expansion never happens, keeping vapor-liquid interface near pin fins. Half of pin fin side walls are covered by thin liquid film to enhance heat transfer.
- CPS condenser has the best performance among the three condensers. It increases heat transfer coefficients by 74% maximally while pressure drops are decreased.
- Future work and comments on phase separation condensers are given in the end of this paper.

Conflict of interest

None declared.

Acknowledgement

Appendix A. Supplementary material

Supplementary data associated with this article can be found, in the online version, at https://doi.org/10.1016/j.ijheatmasstransfer.2017.11.002.

References

[1] H. Chen, J. Xu, Z. Li, F. Xing, J. Xie, W. Wang, W. Zhang, Flow pattern modulation in a horizontal tube by the passive phase separation concept, Int. J. Multiphase Flow 45 (2012) 12–23.
[2] H. Chen, J. Xu, Z. Li, F. Xing, J. Xie, Stratified two-phase flow pattern modulation in a horizontal tube by the mesh pore cylinder surface, Appl. Energy 112 (2013) 1283–1290.
[3] J. Xie, J. Xu, F. Xing, Z. Wang, H. Liu, The phase separation concept condensation heat transfer in horizontal tubes for low-grade energy utilization, Energy 69 (2014) 787–800.
[4] H. Chen, J. Xu, J. Xie, F. Xing, Z. Li, Modulated flow patterns for vertical upflow by the phase separation concept, Exp. Therm. Fluid Sci. 52 (2014) 297–307.
[5] Q. Chen, J. Xu, D. Sun, Z. Cao, J. Xie, F. Xing, Numerical simulation of the modulated flow pattern for vertical upflows by the phase separation concept, Int. J. Multiphase Flow 56 (2013) 105–118.
[6] J. Xie, J. Xu, Y. Cheng, F. Xing, X. He, Condensation heat transfer of R245fa in tubes with and without lyophilic porous-membrane-tube insert, Int. J Heat Mass Transf. 88 (2015) 261–275.
[7] J. Xu, C. Yu, Critical temperature criterion for selection of working fluids for subcritical pressure Organic Rankine cycles, Energy 74 (2014) 719–733.
[8] J.R. Thome, Boiling in microchannels: a review of experiment and theory, Int. J. Heat Fluid Flow 25 (2) (2004) 128–139.
[9] S. Garimella, Condensation flow mechanisms in microchannels: basis for pressure drop and heat transfer models, Heat Transfer Eng. 25 (3) (2004) 104–116.
[10] Y. Chen, P. Cheng, Condensation of steam in silicon microchannels, Int. Commun. Heat Mass Transf. 32 (1–2) (2005) 175–183.
[11] S. Garimella, A. Agarwal, J.D. Killion, Condensation pressure drop in circular microchannels, Heat Transfer Eng. 26 (3) (2005) 28–35.
[12] H.Y. Wu, P. Cheng, Condensation flow patterns in silicon microchannels, Int. J. Heat Mass Transfer 48 (11) (2005) 2186–2197.
[13] W. Zhang, J. Xu, G. Liu, Multi-channel effect of condensation flow in a micro triple-channel condenser, Int. J. Multiphase Flow 34 (12) (2008) 1175–1184.
[14] W. Zhang, J. Xu, J.R. Thome, Periodic bubble emission and appearance of an ordered bubble sequence (train) during condensation in a single microchannel, Int. J. Heat Mass Transfer 51 (13–14) (2008) 3420–3433.
[15] A. Agarwal, S. Garimella, Modeling of pressure drop during condensation in circular and noncircular microchannels, J. Fluid Eng-T. ASME 131 (1) (2009) 011302.
[16] S. Nebuloni, J.R. Thome, Numerical modeling of laminar annular film condensation for different channel shapes, Int. J. Heat Mass Transfer 53 (13–14) (2010) 2615–2627.
[17] S.M. Kim, I. Mudawar, Flow condensation in parallel micro-channels - part 2: heat transfer results and correlation technique, Int. J. Heat Mass Transfer 55 (4) (2012) 984–994.
[18] X. Ma, X. Fan, Z. Lan, R. Jiang, B. Tao, Experimental study on steam condensation with non-condensable gas in horizontal microchannels, Am. Inst. Phys. Conf. Ser., Xian, P.R. China (2013) 146–155.
[19] M.M. Derby, A. Chatterjee, Y. Peles, M.K. Jensen, Flow condensation heat transfer enhancement in a mini-channel with hydrophobic and hydrophilic patterns, Int. J. Heat Mass Transfer 68 (2014) 151–160.
[20] T.M. Zhong, Y. Chen, W.X. Zheng, N. Hua, X.L. Luo, Q.C. Yang, S.P. Mo, L.S. Jia, Experimental investigation on microchannel condensers with and without liquid–vapor separation headers, Appl. Therm. Eng. 73 (2) (2014) 1510–1518.
[21] G. El Achkar, M. Miscevic, P. Lavieille, An experimental study on slug-bubbly condensation flows at low mass velocity in a square-cross-section microchannel, Heat Transfer Eng. 37 (13–14) (2016) 1181–1189.
[22] H. El Mghari, H. Louahlia-Gualous, Experimental and numerical investigations of local condensation heat transfer in a single square microchannel under variable heat flux, Int. Commun. Heat Mass Transfer 71 (2016) 197–207.
[23] X. Dai, F. Yang, R. Fang, T. Yemame, J.A. Khan, C. Li, Enhanced single and two-phase transport phenomena using flow separation in a microgap with copper woven mesh coatings, Appl. Therm. Eng. 54 (1) (2013) 281–288.
[24] S.G. Kandlikar, Enhanced macroconvection mechanism with separate liquid-vapor pathways to improve pool boiling performance, J. Heat Transfer 139 (2017) 051501.
[25] S.G. Kandlikar, Controlling bubble motion over heated surface through evaporation momentum force to enhance pool boiling heat transfer, Appl. Phys. Lett. 102 (2013) 051611.
[26] A. Jaikumar, S.G. Kandlikar, Ultra-high pool boiling performance and effect of channel width with selectively coated open microchannels, Int. J. Heat Mass Transfer 95 (2016) 795–805.
[27] A. Jaikumar, S.G. Kandlikar, Pool boiling enhancement through bubble induced convective liquid flow in feeder microchannels, Appl. Phys. Lett. 108 (4) (2016) 041604.
[28] S. Michielsen, J. Zhang, J. Du, H.J. Lee, Gibbs free energy of liquid drops on conical fibers, Langmuir 27 (19) (2011) 11867–11872.
[29] R. Parmar, S.K. Majumder, Hydrodynamics of microbubble suspension flow in pipes, Ind. Eng. Chem. Res. 53 (9) (2014) 3689–3701.
[30] F.A. Morrison, An Introduction to Fluid Mechanics, Cambridge University Press, New York, 2013.
[31] J.G. Collier, J.R. Thome, convective Boiling and Condensation, third ed., Oxford University Press, Oxford, 1994.
[32] R. Wen, Q. Li, J. Wu, G. Wu, W. Wang, Y. Chen, X. Ma, D. Zhao, R. Yang, Hydrophobic copper nanowires for enhancing condensation heat transfer, Nano Energy 33 (2017) 177–183.
[33] N.A. Patankar, Supernucleating surfaces for nucleate boiling and dropwise condensation heat transfer, Soft Matter 6 (8) (2010) 1613.
[34] V.P. Carey, Liquid-Vapor Phase-Change Phenomena: An Introduction to the Thermophysics of Vaporization and Condensation Processes in Heat Transfer Equipment, Taylor & Francis, Bristol, 1992.
[35] H.J. Cho, D.J. Preston, Y. Zhu, E.N. Wang, Nanoengineered materials for liquid–vapour phase-change heat transfer, Nat. Rev. Mater. 2 (2016) 16092.
[36] Y.Y. Yan, H.C. Lio, T.F. Lin, Condensation heat transfer and pressure drop of refrigerant R134a in a plate heat exchanger, Int. J. Heat Mass Transfer 42 (1999) 993–1006.